NASA Technical Memorandum 103690

IN-07

1604

P.14

Wind Tunnel Wall Effects in a Linear Oscillating Cascade

Daniel H. Buffum
Lewis Research Center
Cleveland, Ohio

and

Sanford Fleeter
Purdue University
West Lafayette, Indiana

Prepared for the
36th International Gas Turbine and Aeroengine Congress and Exposition
sponsored by the American Society of Mechanical Engineers
Orlando, Florida, June 3-6, 1991

NASA

Wind Tunnel Wall Effects in a Linear Oscillating Cascade

Daniel H. Buffum
National Aeronautics and Space Administration
Lewis Research Center
Cleveland, Ohio

Sanford Fleeter
Thermal Sciences and Propulsion Center
School of Mechanical Engineering
Purdue University
West Lafayette, Indiana

ABSTRACT

Experiments in a linear oscillating cascade reveal that the wind tunnel walls enclosing the airfoils have, in some cases, a detrimental effect on the oscillating cascade aerodynamics. In a subsonic flow field, biconvex airfoils are driven simultaneously in harmonic, torsion-mode oscillations for a range of interblade phase angle values. It is found that the cascade dynamic periodicity - the airfoil-to-airfoil variation in unsteady surface pressure - is good for some values of interblade phase angle but poor for others. Correlation of the unsteady pressure data with oscillating flat plate cascade predictions is generally good for conditions where the periodicity is good and poor where the periodicity is poor. Calculations based upon linearized unsteady aerodynamic theory indicate that pressure waves reflected from the wind tunnel walls are responsible for the cases where there is poor periodicity and poor correlation with the predictions.

NOMENCLATURE

C airfoil chord

C_m unsteady aerodynamic moment coefficient, $\int_0^1 (x^*_{ea} - x^*)\Delta C_p(x^*)dx^*$

C_p unsteady pressure coefficient, $p_1/(\rho_{in}V_{in}^2\alpha_1)$

$\bar{C}_p$ steady pressure coefficient, $(\bar{p}_{in} - p_0)/(\rho_{in}V_{in}^2)$

$\hat{C}_p^n$ unsteady pressure influence coefficient for the n^{th} airfoil

$\vec{e}$ unit vector

k reduced frequency, $\omega C/V_{in}$

M_{in} cascade inlet Mach number

N limit of summation

$\bar{p}_{in}$ mean inlet static pressure

p_j j^{th} harmonic of airfoil surface static pressure

S airfoil spacing

V_{in} inlet velocity

x airfoil chordwise coordinate

x^* nondimensional airfoil chordwise coordinate, x/C

x^*_{ea} nondimensional elastic axis location, 1/2

α_j j^{th} harmonic of incidence angle

β interblade phase angle (positive when airfoil n+1 leads airfoil n)

γ stagger angle

ΔC_p unsteady pressure difference coefficient

δC_p dynamic periodicity magnitude difference

$\delta\phi$ dynamic periodicity phase difference

ρ_{in} inlet density

ω airfoil oscillation frequency

INTRODUCTION

Oscillating cascade experiments play an important role in the development of advanced cascade unsteady aerodynamic analyses, providing data used to both evaluate existing analyses and provide direction for future modeling efforts.

Both linear and annular cascades have been used to investigate the aerodynamics of airfoils driven in controlled, harmonic, fixed interblade phase angle traveling-wave mode oscillations. Certain advantages and disadvantages are associated with these two types of facilities. In particular, a highly two-dimensional flow field may be obtained in a linear cascade while, in an annular cascade, undesirable three-dimensional effects may be problematic. However, while the annular cascade appears to be inherently dynamically periodic, i.e., the temporal fluctuations in the flow field vary from passage to passage according to the interblade phase angle, periodicity is less certain in the linear cascade due to the finite extent of the cascade and the boundaries introduced by the wind tunnel walls. The potential for wall interference is indicated by a number of papers devoted to the effects of wind tunnel walls on a single oscillating airfoil, for example, Jones (1943) and Runyan et al. (1955).

Carta (1983) was the first researcher to investigate the dynamic periodicity of a linear oscillating cascade. His cascade consisted of 11 NACA 65-series airfoils staggered at 30 degrees with 1.33 solidity. Airfoil surface unsteady pressures were measured at reduced frequency values ranging from 0.14 to 0.30 over a wide range of interblade phase angles with a low subsonic inlet Mach number, $M \approx 0.18$. Good dynamic periodicity was generally found except for in-phase oscillations, where circumferential gradients in the phase of the unsteady pressure coefficient were found. Carta attributed this to an acoustic resonance condition in the cascade.

In the present study, the steady and unsteady aerodynamics of an oscillating, linear cascade are investigated in a low solidity configuration. The cascade solidity, 0.65, was chosen to be representative of an advanced propeller model which fluttered during wind tunnel performance tests (Mehmed et al., 1982). For an inlet Mach number of 0.55, the torsion mode biconvex airfoil oscillating cascade aerodynamics are quantified for reduced frequencies as high as 0.64 and a range of interblade phase angles. To help determine the validity of the data, an investigation is made into the steady state and dynamic periodicity of the cascade. Then the unsteady airfoil surface pressure data are correlated with the predictions of the linearized subsonic oscillating cascade analysis of Smith (1972). Insight into the effect of the wind tunnel walls on the cascade unsteady aerodynamics is gained from the theoretical acoustic wave generation properties of an oscillating cascade.

OSCILLATING CASCADE FACILITY

The NASA Lewis Transonic Oscillating Cascade, Figure 1, combines a linear cascade wind tunnel capable of inlet flow approaching Mach one with a high-speed airfoil drive system which imparts torsion-mode oscillations to the cascaded airfoils at specified interblade phase angles and realistic high reduced frequency values.

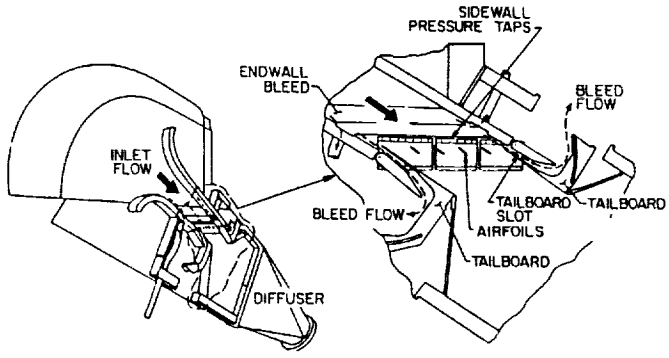

Figure 1 Oscillating cascade facility

Air drawn from the atmosphere passes through a smooth contraction inlet section into a constant area rectangular test section of 9.78 cm span which measures 58.6 cm along the stagger line. Upstream of the test section, suction is applied through perforated walls to reduce the boundary layer thickness. Tailboards are used to adjust the cascade exit region static pressure and also form bleed scoops which further reduce upper and lower wall boundary layer effects. Downstream of the test section, the air is expanded through a diffuser into an exhaust header. The exhaust system, part of a central air facility at Lewis, maintains a 30 kPa pressure downstream of the flow control valves. The cascade inlet and the airfoil angles may be adjusted over a wide range of incidence and stagger angle combinations.

The facility features a high-speed mechanism which drives the four airfoils in controlled torsional oscillations. Four stainless steel barrel cams, each having a six cycle sinusoidal groove machined into its periphery, are mounted on a common rotating shaft driven by a 74.6 kW electric motor. A cam follower assembly, consisting of a titanium alloy connecting arm with a stainless steel button on one end, is joined on the other end to an airfoil trunnion. The button fits into the cam groove, thus coupling the airfoil to the camshaft. Lubrication of the cam/follower assembly is provided by an oil bath. The amplitude of the torsional airfoil motion is 1.2 degrees as dictated by the cam and follower geometry. The drive system is configured for oscillations at a chosen interblade phase angle by fixing the cams at the required relative positions on the shaft. A reduced frequency of 0.64 is achieved at 0.55 inlet Mach number with an oscillation frequency of 250 Hz.

AIRFOILS AND INSTRUMENTATION

Figure 2 illustrates the airfoil and cascade geometry which is summarized in Table 1. Four uncambered, 7.6% thick biconvex airfoils are used to create a low solidity ($C/S = 0.65$) cascade. The stagger angle is 45 degrees and the airfoils oscillate about the midchord.

Airfoils instrumented with static pressure taps are used to measure the airfoil surface steady pressure distributions. There are sixteen chordwise measurement locations, with a higher density in the leading edge region used to capture the higher gradients there. Rows of sidewall static pressure taps located upstream and downstream of the cascaded airfoils are used to determine the mean inlet and exit pressures.

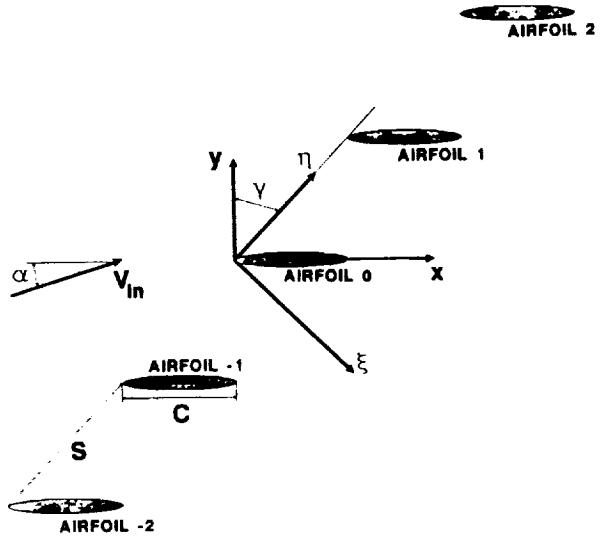

Figure 2 Cascade geometry

Table 1 Airfoil and cascade geometry

Airfoil	
Type	biconvex, no camber
Surface radius of curvature	27.4 cm
Leading and trailing edge radii of curvature	0.025 cm
Chord, C	7.62 cm
Maximum thickness / chord	0.076
Elastic axis	midchord
Dynamic pressure transducer locations, % chord	12,25,40,60,75,88
Cascade	
Number of airfoils	4
Airfoil spacing, S	11.72 cm
Solidity, C/S	0.65
Stagger angle, γ	45 degrees
Mean flow incidence angle, α_0	2 degrees
Amplitude of oscillation, α_1	1.2 degrees

Flush-mounted high-frequency-response miniature pressure transducers are used to measure the unsteady surface pressures on the oscillating airfoils. Two airfoils are instrumented, each having six transducers mounted symmetrically about the midchord on one airfoil surface. These transducers, having active sensor diameters of 1.3% of the airfoil chord, are epoxied into milled slots and potted in room-temperature-vulcanizing rubber for isolation from airfoil strain. A thin coating of rubber is also used to fair the transducer surface into the airfoil contour.

From static and dynamic calibrations, the pressure transducers were found to be highly linear in response over the frequency and pressure ranges of interest. However, the pressure transducers may produce undesirable signals as a consequence of the airfoil motion. This effect was quantified by oscillating the instrumented airfoils under no-flow conditions. The response of each transducer was found to be a linear function of the airfoil acceleration, implying that the acoustic response, which varies with the airfoil velocity magnitude, is dominated by the acceleration response. Thus calibration data were obtained to correct the oscillating airfoil pressure data for acceleration effects.

The time-variant position of the reference oscillating airfoil is determined by a capacitance-type proximity sensor which produces a voltage proportional to the air gap between it and an adjacent object. This sensor is positioned to face a six cycle sinusoidally-shaped cam mounted on the airfoil drive camshaft so as to be in phase with the reference airfoil motion.

DATA ACQUISITION AND ANALYSIS

Conventional instrumentation is used to quantify the steady flow field. An average of the upstream sidewall static pressures along with the atmospheric pressure (total) are used to calculate the inlet Mach number. Steady flow airfoil surface static pressures are calculated from an average of approximately 100 samples. The steady pressure coefficient is defined in Equation 1.

$$\bar{C}_p(x) = \frac{p_{in} - p_0(x)}{\rho_{in} V_{in}^2} \qquad (1)$$

p_{in} is the mean inlet static pressure, p_0 is the time-average airfoil surface static pressure at the chordwise coordinate x, and ρ_{in} and V_{in} are the inlet values of density and velocity.

Unsteady signals are recorded on magnetic tape for post-experiment processing. During tape playback, the signals are simultaneously digitized at rates sufficient to capture at least three harmonics of the oscillation frequency, with 32,768 samples taken per channel. Each channel of data is divided into contiguous blocks, each block typically with 2048 samples, and then Fourier decomposed to determine the first harmonic of each block of data. The first harmonic pressure of each block is referenced to the airfoil motion by subtracting from it the phase of the first harmonic motion signal of the same block. Once all of the blocks from a channel are decomposed in this manner, the first harmonic block results are averaged and the complex-valued acceleration response is subtracted vectorally. Statistical analysis of the block results is used to estimate uncertainties for the average first harmonic values.

In these experiments, the motion of the n^{th} airfoil is defined by the change in the incidence angle with time:

$$\alpha^n(t) = \alpha_0 + \alpha_1 \Re\{e^{i(\omega t - n\beta)}\} \qquad (2)$$

where α_0 is the mean incidence angle, α_1 is the torsional oscillation amplitude, ω is the frequency, β is the interblade phase angle and $\Re$ denotes the real part.

The complex-valued unsteady pressure coefficient is defined as

$$C_p(x) = \frac{p_1(x)}{\rho_{in} V_{in}^2 \alpha_1}. \qquad (3)$$

p_1 is the first harmonic airfoil surface static pressure. The dynamic pressure difference coefficient is the difference between the lower and upper surface unsteady pressure coefficients:

$$\Delta C_p = C_{pl} - C_{pu}. \qquad (4)$$

LINEARIZED ANALYSIS

The experimental dynamic pressure difference coefficient data are correlated with the predictions of a computer program published by Whitehead (1987) which is based on the analysis of Smith (1972). This is a semi-analytical technique for determining the unsteady forces on an infinite cascade of flat plate airfoils subject to harmonic disturbances in an inviscid, isentropic, subsonic, unsteady flow. The analysis assumes that the airfoils are at zero mean incidence and the unsteadiness creates small disturbances to a uniform mean flow, resulting in a linear system of equations with constant coefficients. Additional analytical results which will be used in the results section are derived below.

Wave Generation by an Oscillating Cascade

The linearized conservation equations for mass and momentum may be expressed as

$$\frac{\partial \mathbf{q}}{\partial t} + \mathrm{A}\frac{\partial \mathbf{q}}{\partial \xi} + \mathrm{B}\frac{\partial \mathbf{q}}{\partial \eta} = 0 \qquad (5)$$

where $\mathbf{q}$ is the matrix of perturbation variables

$$\mathbf{q} = \begin{pmatrix} p_1 \\ u_1 \\ v_1 \end{pmatrix} \qquad (6)$$

and the coefficient matrices A and B are constant, depending on the uniform mean flow.

$$\mathrm{A} = \begin{pmatrix} u_0 & \rho_0 a_0^2 & 0 \\ 1/\rho_0 & u_0 & 0 \\ 0 & 0 & u_0 \end{pmatrix} \qquad (7)$$

$$\mathrm{B} = \begin{pmatrix} v_0 & 0 & \rho_0 a_0^2 \\ 0 & v_0 & 0 \\ 1/\rho_0 & 0 & v_0 \end{pmatrix} \qquad (8)$$

u_0 and v_0 are the ξ and η components of the mean flow velocity, ρ_0 is the mean density and a_0 is the mean speed of sound.

For an infinite cascade of equally-spaced airfoils oscillating harmonically at a fixed interblade phase angle, the dependent variables depend harmonically on the spatial position and time. Thus the perturbations are expressed as

$$\mathbf{q} = \begin{pmatrix} p_1 \\ u_1 \\ v_1 \end{pmatrix} = \begin{pmatrix} \bar{p}_1 \\ \bar{u}_1 \\ \bar{v}_1 \end{pmatrix} e^{i(\omega t + l\xi + m\eta)} = \bar{\mathbf{q}} e^{i(\omega t + l\xi + m\eta)} \qquad (9)$$

where l and m are the axial and circumferential wavenumbers and the quantities with overbars are complex.
Substituting these perturbation expressions into Equation 5 and differentiating results in

$$(\omega \mathrm{I} + l\mathrm{A} + m\mathrm{B})\bar{\mathbf{q}} = 0 \qquad (10)$$

where I is the identity matrix.

Equation 10 may be rearranged in the form of an eigenvalue problem, Equation 11, with the axial wavenumber l being the eigenvalue.

$$(-\mathrm{A}^{-1}(\omega \mathrm{I} + m\mathrm{B}) - l\mathrm{I})\bar{\mathbf{q}} = 0 \qquad (11)$$

The eigenvalues are

$$l = \frac{-(\omega + m v_0)}{u_0} \qquad (12)$$

and

$$l = \frac{u_0(\omega + v_0 m) \pm a_0\sqrt{(\omega + v_0 m)^2 - (a_0^2 - u_0^2)m^2}}{a_0^2 - u_0^2}. \qquad (13)$$

As shown by Smith, the first eigenvalue, Equation 12, corresponds to convection of vorticity by the mean flow with no associated pressure fluctuations. This solution is of no further interest for this application. However, the eigenvalues of Equation 13, corresponding to irrotational pressure perturbations, are of interest.

The tangential wave number must satisfy cascade dynamic periodicity according to the interblade phase angle β. Hence

$$mS = \beta + 2\pi r \qquad (14)$$

where S is the cascade spacing and r is an integer specifying the mode of the wave.

The nature of the acoustic waves produced by the cascade depends upon the term under the radical in Equation 13. Let δ be that term:

$$\delta = (\omega + v_0 m)^2 - (a_0^2 - u_0^2)m^2. \qquad (15)$$

When $\delta = 0$, the acoustic resonance condition, only one wave is created which propagates in the circumferential direction. The resonant values of the interblade phase angle are determined by solving Equation 15, with $\delta = 0$, for m, then using Equation 14 to determine β for $r=0$. The result is:

$$\beta_r^* = \frac{2kMS}{C(1 - M^2)}\left(M\sin(\alpha_0 + \gamma) \pm \sqrt{1 - M^2\cos^2(\alpha_0 + \gamma)}\right). \qquad (16)$$

When $\delta > 0$, both values of l as specified by Equation 13 are real, thus there are two acoustic waves which propagate undiminished, one going upstream and the other downstream. This behavior is termed superresonant when the mean flow field is subsonic.

The final case is $\delta < 0$, the subsonic cascade subresonant condition. l is now complex, and may be expressed as $l = l^R + il'$ with the real and imaginary parts determined from Equation 13 to be

$$l^R = \frac{u_0(\omega + v_0 m)}{a_0^2 - u_0^2} \tag{17}$$

and

$$l' = \frac{\pm a_0 \sqrt{|(\omega + v_0 m)^2 - (a_0^2 - u_0^2)m^2|}}{a_0^2 - u_0^2}. \tag{18}$$

In this case, the pressure perturbation is of the form

$$p_1 = \overline{p}_1 e^{i(\omega t - (l^R + il')\xi + m\eta)}$$

$$= \overline{p}_1 e^{-l'\xi} e^{i(\omega t - l^R \xi + m\eta)} \tag{19}$$

Thus the wave decays exponentially with ξ, depending upon the imaginary part of l:

$$\frac{|p_1(\xi)|}{|\overline{p}_1|} = e^{-|l'\xi|} \tag{20}$$

where, from Equation 19, $|\overline{p}_1|$ is equal to $|p_1(\xi = 0)|$. The absolute value of the exponent disallows the non-physical case of an amplifying wave.

The axial and tangential wave numbers specify the acoustic wave propagation direction relative to ξ', η' coordinates which are parallel to the fixed ξ, η coordinate system but moving with the mean flow velocity (Whitehead, 1987). Relative to the ξ', η' coordinates, the waves propagate at the angle

$$\theta' = \tan^{-1}\left(\frac{\mp m}{-l^R}\right) \tag{21}$$

with the speed of sound. The wave propagation vector V_p in the ξ, η coordinate system is therefore the sum of the steady flow velocity vector and the wave propagation vector relative to the moving coordinate system,

$$V_p = (u_0 + a_0 \cos\theta')\vec{e}_\xi + (v_0 + a_0 \sin\theta')\vec{e}_\eta. \tag{22}$$

It follows that the direction of propagation θ in the ξ, η coordinate system is

$$\theta = \tan^{-1}\left(\frac{v_0 + a_0 \sin\theta'}{u_0 + a_0 \cos\theta'}\right). \tag{23}$$

Influence Coefficient Technique

In this analysis, the superposition principle is valid since the system of governing small disturbance equations is linear. The unsteady pressure difference coefficient on a reference airfoil (airfoil 0) for fixed values of the inlet Mach number, reduced frequency and cascade geometry may be expressed as the sum of the effects of the oscillations of the reference airfoil itself and the other airfoils in the cascade, Equation 24.

$$\Delta C_p(x, \beta) = \sum_{n=-N}^{N} \Delta \hat{C}_p^n(x) e^{in\beta} \tag{24}$$

where the complex-valued influence coefficient $\Delta \hat{C}_p^n$ expresses the influence that the oscillations of airfoil n have on the pressure difference coefficient of the reference airfoil. $N = \infty$ for an infinite cascade.

By inversion of Equation 24, an expression for the influence coefficients is

$$\Delta \hat{C}_p^n(x) = \frac{1}{2\pi} \int_{-\pi}^{\pi} \Delta C_p(x, \beta) e^{-in\beta} d\beta. \tag{25}$$

Unsteady aerodynamic influence coefficients may thus be determined from oscillating cascade analyses by integrating the analytical predictions over the complete interblade phase angle interval. Using these influence coefficients for a finite value of N in Equation 24 then enables analytical results for a finite number of airfoils oscillating in an infinite cascade to be determined.

RESULTS

The effect of wind tunnel walls on the aerodynamics of a low solidity linear oscillating cascade is investigated using experimental and analytical techniques. For a mean inlet Mach number of 0.55 and 2 degrees mean incidence, the airfoil surface steady pressure coefficient distributions are presented first, followed by dynamic periodicity data and correlation of the unsteady pressure difference coefficient data with linearized analysis predictions. Linearized analysis is then used to ascertain the effects of the wind tunnel walls on the cascade unsteady aerodynamics.

Steady State Aerodynamics

For a linear cascade to be a valid simulation of a turbomachine blade row, the cascade must exhibit good passage-to-passage periodicity for the steady flow field. Thus airfoil surface steady pressure distributions are obtained for multiple passages in the low solidity cascade. In Figure 3, steady pressure coefficient data are presented for the center cascade

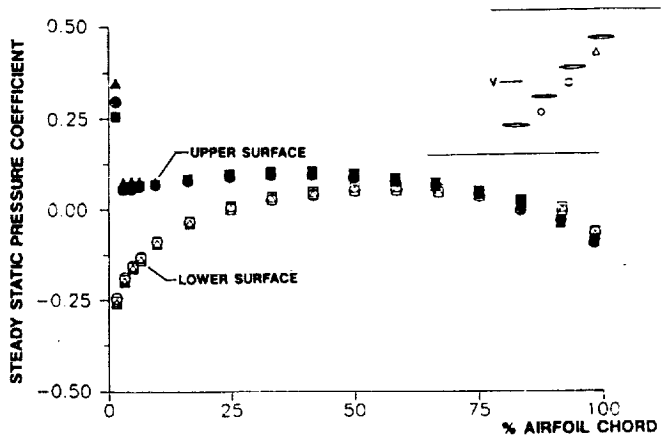

Figure 3 Airfoil surface steady pressure coefficient distributions, M=0.55, α_0=2 degrees

passage and the two adjacent passages. Good cascade periodicity is apparent, with the only significant differences found at the leading edge of the airfoil upper surface.

The upper surface pressure coefficient distribution peaks near the leading edge and the pressure difference tends toward zero near the trailing edge. There is negligible loading beyond 50% of chord. Using the method of Kline and McClintock (1953), a 95% confidence interval of ±0.003 is estimated for these pressure coefficients. The mean exit region static pressure divided by the inlet total pressure was 0.8251.

Unsteady Aerodynamics

Figure 4 illustrates typical subsonic cascade behavior in terms of the wave propagation modes predicted by the linearized analysis. Acoustic resonances at positive and negative interblade phase angle values, β_r^*, bracket the

k	β_r^-	β_r^+
0.40	-14.6	37.0
0.64	-23.3	59.1

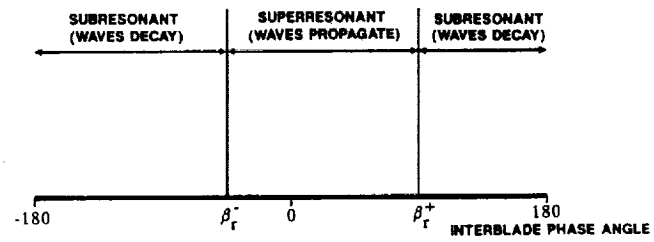

Figure 4 Modes of subsonic oscillating cascade wave propagation

wave-propagating superresonant region which includes $\beta = 0$. When $\beta > \beta_r^+$ or $\beta < \beta_r^-$, the cascade is subresonant and the waves decay. Included in this figure are the resonant values of interblade phase angle, Equation 16, for the experimental conditions.

The unsteady aerodynamic experiments discussed herein include subresonant and superresonant values of β. Airfoil surface unsteady pressure distributions are obtained for interblade phase angle values of 0, 45, -45, 90, -90 and 180 degrees at reduced frequency values of 0.40 and 0.64. Sample

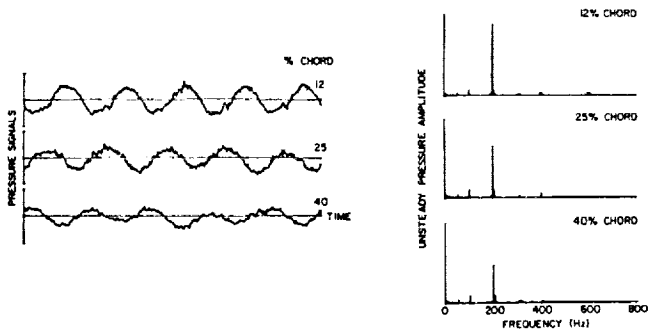

Figure 5 Time-variant signals and averaged pressure spectra

time-variant pressure signals presented in Figure 5 along with the resulting pressure spectra illustrate the dominance of the first harmonic component as typically found in the signals. 95% confidence intervals of ± 5% in magnitude and ±3 degrees in phase are estimated for the mean value of the unsteady pressure coefficients.

Dynamic Periodicity. Oscillating cascade data were first obtained by positioning the two instrumented airfoils to measure the unsteady pressures on the airfoil surfaces which define the center passage of the cascade. The dynamic periodicity of the cascade was investigated by subsequently positioning the instrumented airfoils to measure the opposite surfaces of the two center airfoils positions, thus giving dynamic pressure measurements for both surfaces of the two most centrally located airfoils.

First harmonic unsteady pressure coefficient periodicity data are presented in Figure 6 for k=0.40 and β=-45 degrees. To

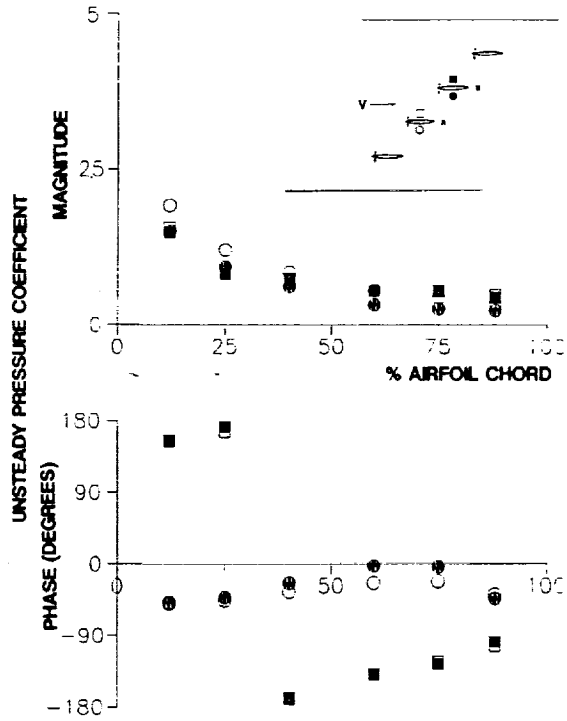

Figure 6 Cascade dynamic periodicity, k=0.40, β= -45 degrees

simplify the discussion of these results, the two instrumented airfoils will be referred to as A and B as labeled in the figure. The data indicate that the dynamic periodicity is excellent in both magnitude and phase for the airfoil upper surface. Although the lower surface periodicity is good, the magnitudes tend to be larger on airfoil A, particularly over the forward half of the airfoil. There are also small but noticeable phase differences in the midchord region on the lower surface.

To aid the presentation of the periodicity data, two new quantities are defined. The dynamic periodicity magnitude and phase differences, δC_p and $\delta\phi$, are defined in Equations 26

and 27 for each airfoil surface. Ideally, both of these quantities will be zero.

$$\delta C_p = \frac{|C_p^A| - |C_p^B|}{\frac{1}{2}(|C_p^A| + |C_p^B|)_{x/C=0.12}} \qquad (26)$$

$$\delta\phi = \phi_p^A - \phi_p^B \qquad (27)$$

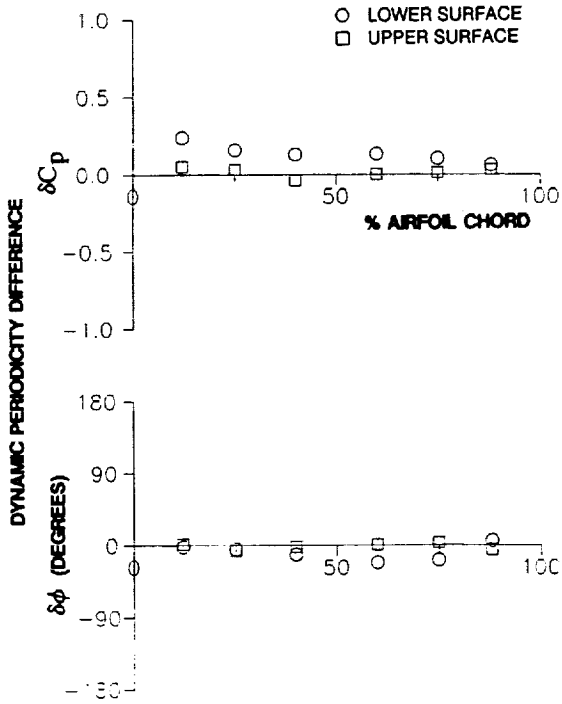

Figure 7 Dynamic periodicity difference, k=0.40, β= -45 degrees

Figure 7 presents the dynamic periodicity data determined from the data presented in Figure 6. Both the excellent upper surface periodicity and defects in the lower surface periodicity are clearly revealed.

The oscillating cascade periodicity is now investigated as a function of reduced frequency and interblade phase angle using the quantities δC_p and $\delta\phi$. Reduced frequency crossplots of the periodicity data for k=0.40 and 0.64 are presented in Figures 8 through 13 for several values of interblade phase angle. Beginning with $\beta = 0°$, Figure 8, the dynamic periodicity is generally poor in both magnitude and phase for these superresonant conditions, and reduced frequency has little effect on the results. The dynamic periodicity is improved somewhat for $\beta = 45°$, Figure 9, but the small values of $\delta\phi$ occurring over the forward half of the airfoil are in contrast to the very large values of $\delta\phi$ at 60 and 75% of chord on the upper surface. Reduced frequency again has little effect on the results even though k=0.40 corresponds to a subresonant condition and k=0.64 is superresonant. In contrast, the periodicity is generally good for $\beta = -45°$, Figure 10, where both reduced frequencies are subresonant. There, all of the values of $\delta\phi$ are

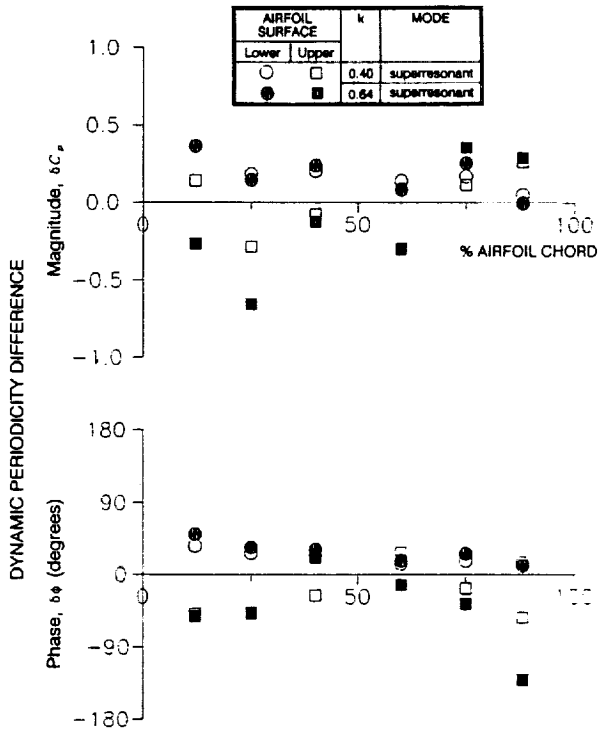

Figure 8 Dynamic periodicity difference, β= 0

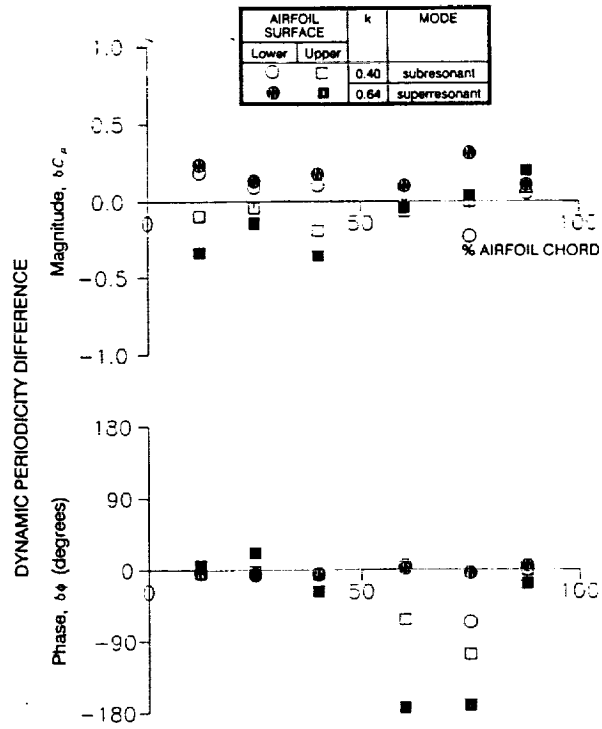

Figure 9 Dynamic periodicity difference, β= 45 degrees

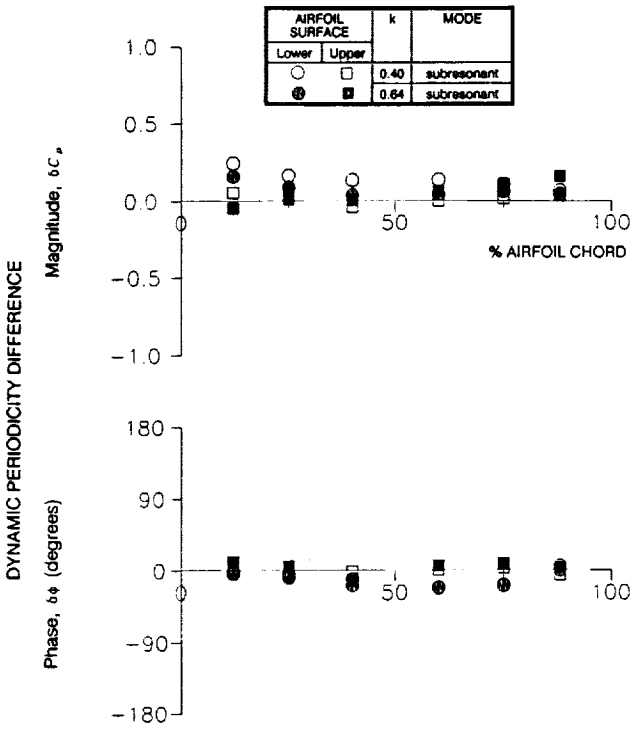

Figure 10 Dynamic periodicity difference, β= -45 degrees

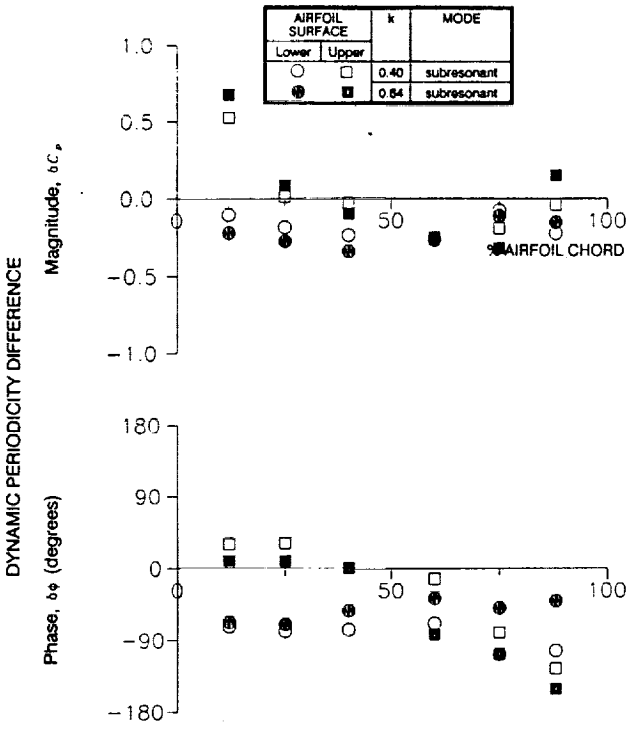

Figure 11 Dynamic periodicity difference, β= 90 degrees

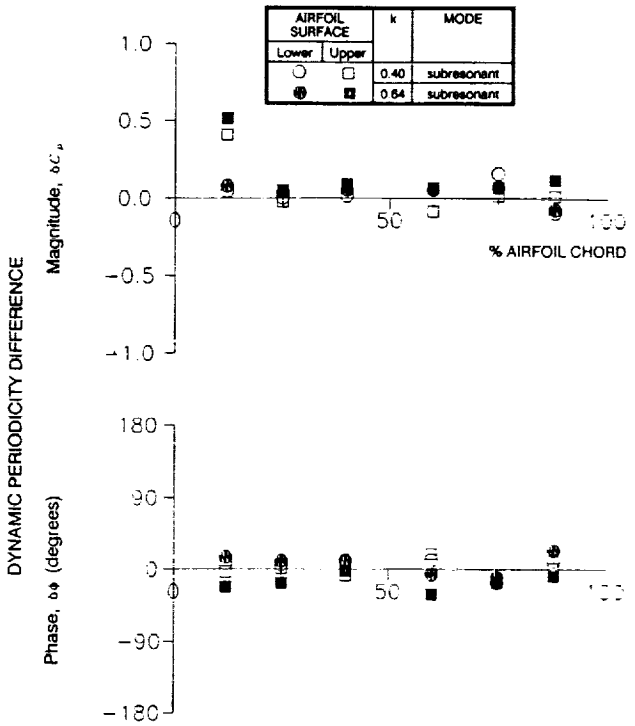

Figure 12 Dynamic periodicity difference, β= -90 degrees

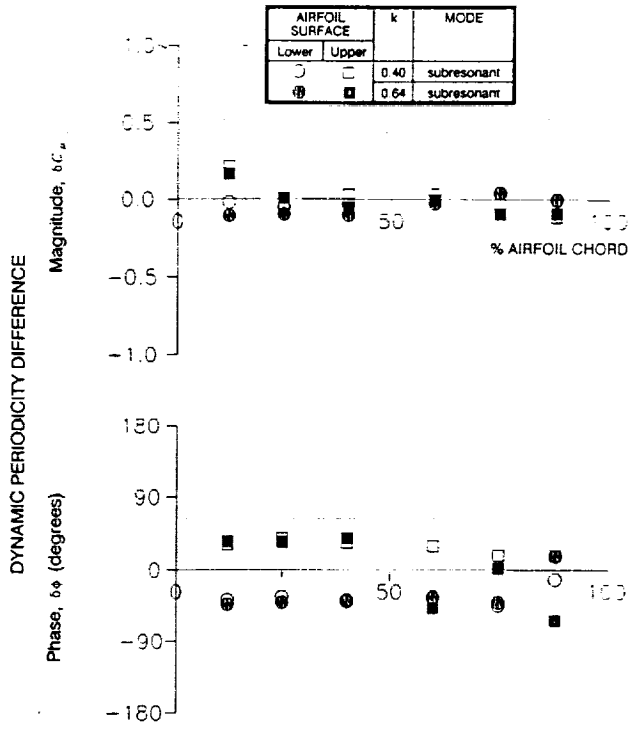

Figure 13 Dynamic periodicity difference, β= 180 degrees

acceptably small as are the values of δC_p except for the lower surface k=0.40 results. When $\beta = 90°$, the periodicity is poor in both magnitude and phase for both subresonant conditions, Figure 11. But for $\beta = -90°$, Figure 12, dynamic periodicity is generally good for these subresonant conditions except for the upper surface magnitude difference at 12% of chord. Finally, for out-of-phase oscillations (subresonant), Figure 13, the magnitude differences are small, but the phase differences are not. Again, reduced frequency has little effect on the results.

To summarize these data, the dynamic periodicity is largely a function of the interblade phase angle, and the periodicity is acceptable only for $\beta = -45°$ and $\beta = -90°$. For both values of reduced frequency, these values of β are predicted to be subresonant. However, subresonance does not guarantee good dynamic periodicity: for example, the periodicity is poor for $\beta = 90°$, a subresonant value of the interblade phase angle for both values of reduced frequency.

Correlation with Linearized Analysis. The experimental dynamic pressure difference coefficient data are correlated with the predictions of the linearized unsteady cascade analysis for an infinite number of airfoils. In addition to the infinite cascade predictions, influence coefficient predictions for the effects of 5 oscillating airfoils ($N=2$ in Equation 24) will be presented.

For a reduced frequency of 0.64 and a range of interblade phase angle values, Figures 14 through 19 present correlations of the experimentally-determined airfoil surface unsteady pressure difference coefficient distributions with the linearized analysis predictions. For conditions where the cascade dynamic periodicity is good, $\beta = -45°$ and $\beta = -90°$, the correlations between the analytical results and the experimental data are good, Figures 14 and 15. Conversely, the data-analysis correlations are generally poor for conditions where the periodicity is poor, $\beta = 45°, 90°$ and $180°$, Figures 16 through 18. At those conditions, the phase angle data-analysis correlation is consistently poor, with the experimentally-determined phases leading the predictions except near the trailing edge. An exception is $\beta = 0°$, Figure

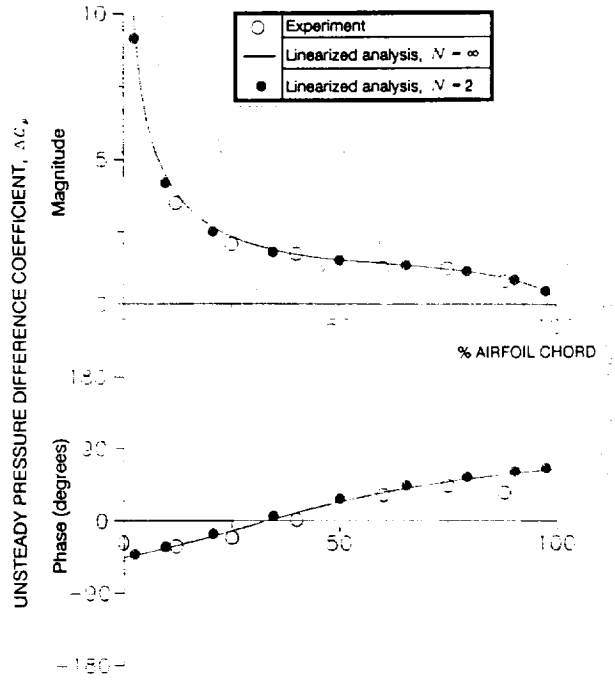

Figure 15 Unsteady pressure difference coefficient distribution, k=0.64, β= -90 degrees

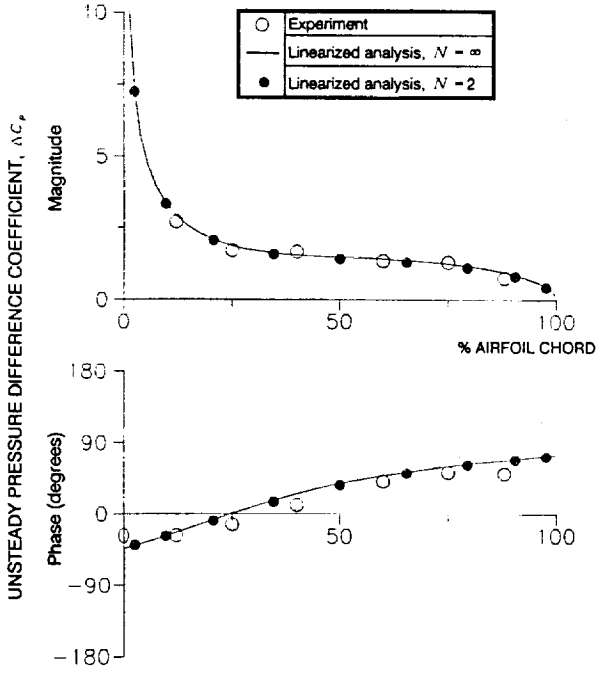

Figure 14 Unsteady pressure difference coefficient distribution, k=0.64, β= -45 degrees

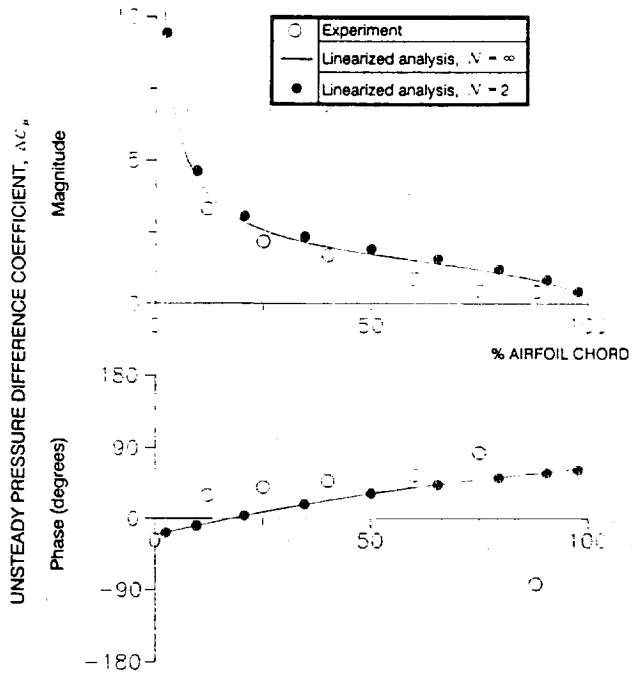

Figure 16 Unsteady pressure difference coefficient distribution, k=0.64, β= 45 degrees

19, for which the data-analysis correlation is good despite poor dynamic periodicity.

The analytical influence coefficient predictions for N =2 are generally in very good agreement with the predictions for an infinite cascade. This indicates that only a few oscillating airfoils are required to model an infinite cascade under these conditions. To consider this further, the imaginary part of the unsteady aerodynamic moment coefficient is presented as a function of interblade phase angle in Figure 20. Linearized analysis results are shown for $N = \infty$, N =6 and N =2. The predictions for N =2 and N =6 are in very good agreement with the infinite cascade results except in the vicinity of the acoustic resonances. At those points, a large number of terms in the Fourier series are required to describe the rapidly changing moment coefficient. This indicates that acoustic resonances will not occur in linear oscillating cascade experiments due to the limited number of airfoils.

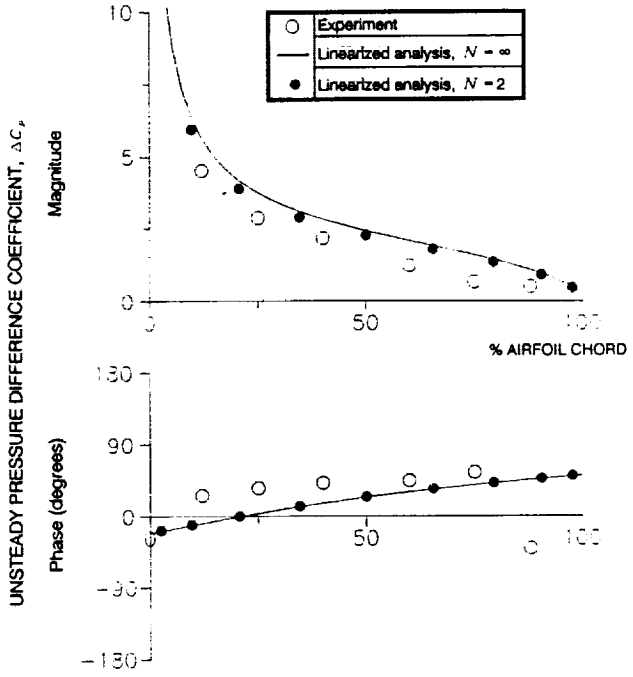

Figure 17 Unsteady pressure difference coefficient distribution, k=0.64, β= 90 degrees

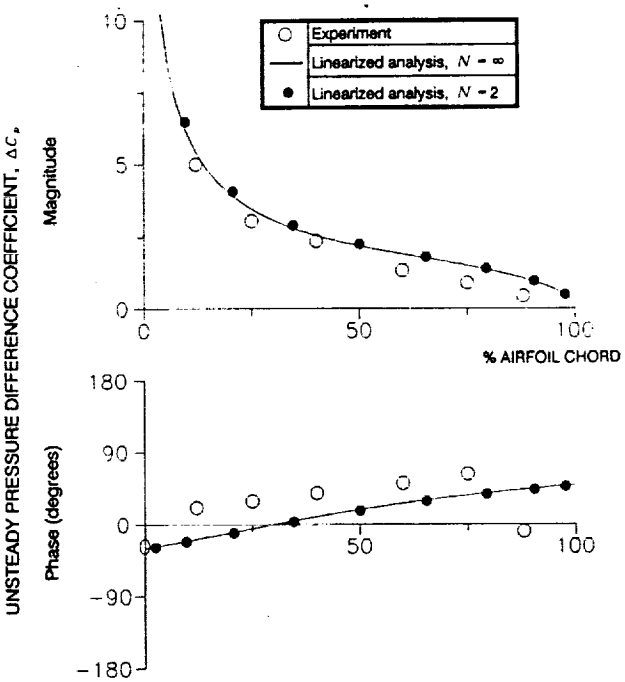

Figure 18 Unsteady pressure difference coefficient distribution, k=0.64, β= 180 degrees

Wind Tunnel Wall Effects. The cascade dynamic periodicity and correlation of the experimental data with the linearized analysis have been shown to vary greatly with

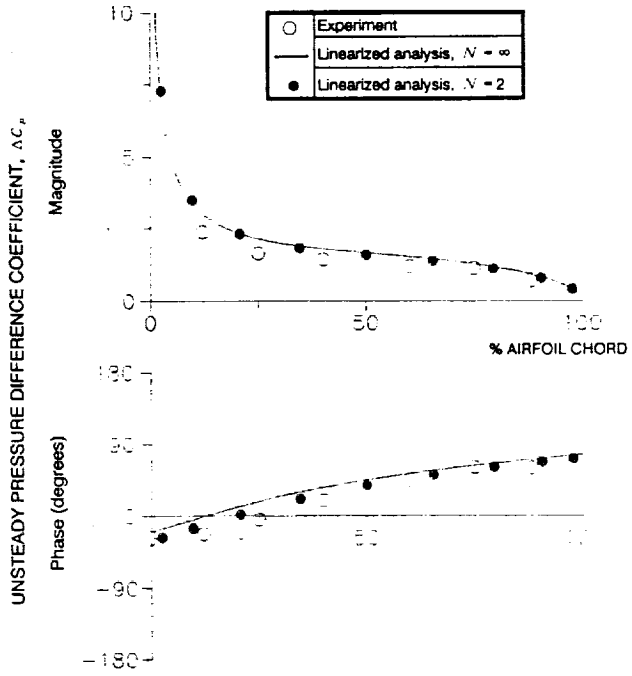

Figure 19 Unsteady pressure difference coefficient distribution, k=0.64, β= 0

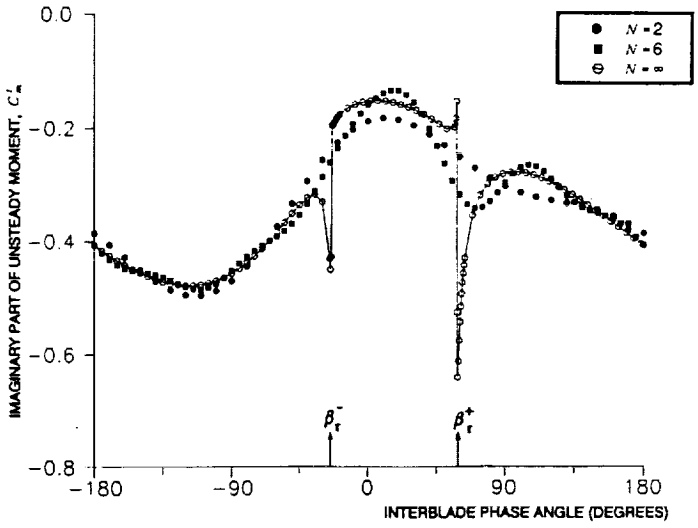

Figure 20 Imaginary part of unsteady aerodynamic moment coefficient as predicted by linearized analysis

interblade phase angle. How these correlations can be very good for some interblade phase angles but poor for others leads one to question the effects of the wind tunnel walls on these results. In this section, linearized analysis is used to gain insight into oscillating cascade/wind tunnel wall interactions.

The calculated direction of acoustic wave propagation θ is shown in Figure 21 for the low solidity cascade geometry with

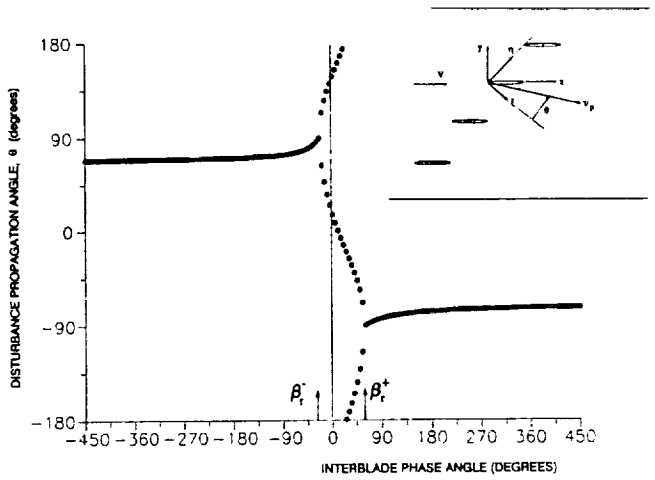

Figure 21 Pressure disturbance propagation direction

M=0.55 and k=0.64. For any one value of β in the superresonant region, two waves are produced, one traveling upstream (in the -ξ direction) and the other going downstream (in the ξ direction). Outside this region, the oscillating cascade produces subresonant waves which travel downstream. Acoustic resonances occur at the boundaries between the subresonant and superresonant regions, with pressure disturbances propagating along the cascade in the $\pm\eta$ directions.

Values of the initial magnitude of the outgoing pressure disturbance, computed using Whitehead's computer program, are presented in Figure 22 in the format of an unsteady pressure coefficient magnitude at the leading edge of the cascade, $|C_p(\xi = 0)|$. Peaks in the largest initial disturbance amplitudes are found in the vicinity of the acoustic resonances, $\beta = \beta_r^*$. Outside the near-resonance regions, relatively large amplitudes occur at positive subresonant values of the interblade phase angle, $\beta > \beta_r^*$, but in general the amplitudes are of the same order of magnitude throughout the interblade phase angle range.

The disturbances will propagate or decay exponentially with distance from the cascade according to the imaginary part of the axial wavenumber, l', Equation 20. As shown in Figure 23, $l' = 0$ in the superresonant region, hence superresonant disturbances propagate away from the cascade without attenuation. Outside this region, l' is nonzero and increases monotonically with $|\beta|$, thus the subresonant waves decay exponentially with distance away from the cascade.

Now the interaction of the predicted waves with the wind tunnel walls is considered. For $\beta = -45°$ and $\beta = -90°$, interblade phase angles where the data-analysis correlation is

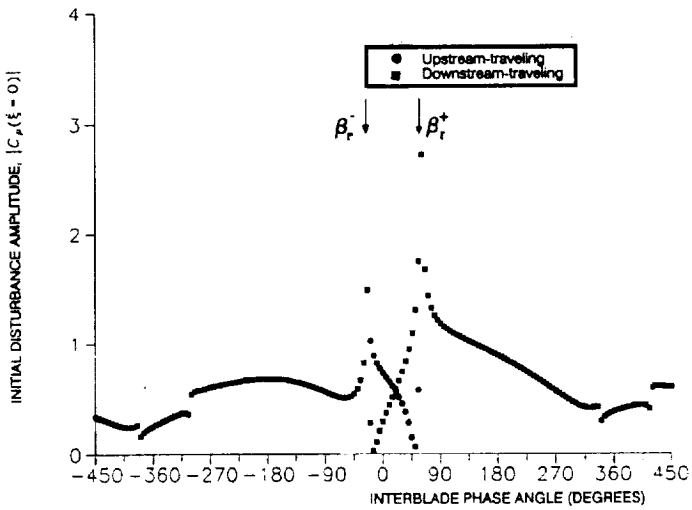

Figure 22 Initial pressure disturbance amplitude

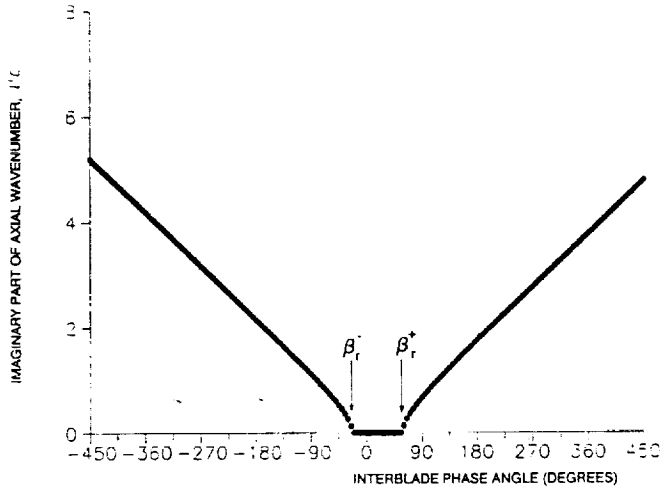

Figure 23 Imaginary part of axial wavenumber

good, decaying waves traveling at $\theta \approx 81°$ with $|C_p(\xi = 0)| \approx 0.5$ are predicted. As shown in the schematic of Figure 24, these waves are directed at the cascade upper wall. The waves are assumed to reflect specularly from the wall so that the reflected disturbances propagate away from the cascade and thus will have no effect on the oscillating cascade aerodynamics.

The data-analysis correlation is also good for $\beta = 0°$, a superresonant condition, but this is considered fortuitous because the cascade periodicity is poor. The upstream-traveling wave for this condition, Figure 24, is directed at the cascade upper wall so that reflected waves travel back into the cascade and potentially affect the cascade unsteady aerodynamics and dynamic periodicity.

The data-analysis correlation is poor for $\beta = 45°$, the other superresonant condition. In this case, the downstream-traveling wave is predicted to interfere with the cascade after reflection off the lower wind tunnel wall, Figure 24.

Decaying waves are predicted for $\beta = 90°$ and $\beta = 180°$, interblade phase angles for which there is poor correlation

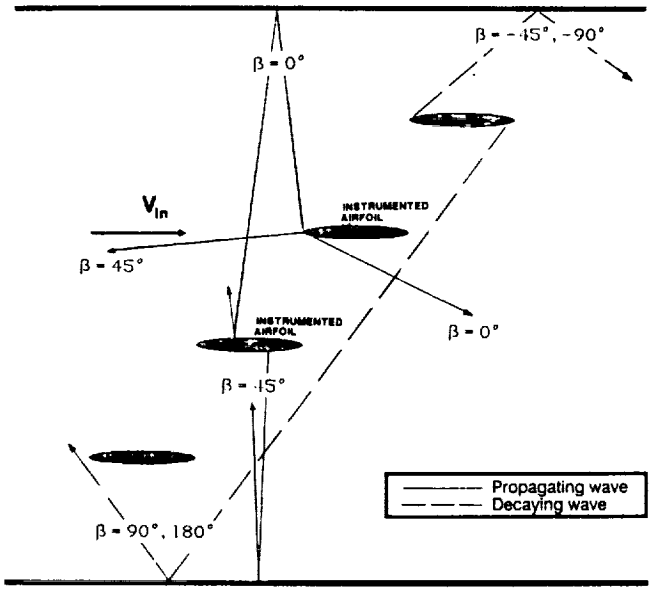

Figure 24 Interaction of pressure disturbances with wind tunnel walls

between the data for all airfoils oscillating and the theory. Despite the poor correlation, the waves are predicted to reflect off the lower wind tunnel wall and propagate upstream without intersecting an airfoil, Figure 24. This discrepancy may be due to limitations of the linearized analysis, in particular, the assumption of a uniform mean flow.

SUMMARY AND CONCLUSIONS

Steady and unsteady airfoil surface pressure distributions have been obtained in a low solidity linear cascade oscillating at reduced frequencies up to 0.64 with 0.55 inlet Mach number. The airfoils were driven in simultaneous torsion-mode oscillations for a range of interblade phase angles. Steady and unsteady airfoil surface pressure distributions were measured, the latter using flush-mounted miniature pressure transducers. Discrete Fourier analysis techniques were used to analyze the unsteady pressure data and determine the first harmonic components. Periodicity of the cascade was determined by measuring the steady and unsteady pressures on the airfoil surfaces defining the two passages at the center of the cascade. The unsteady pressure difference coefficient data were correlated with flat plate cascade predictions. In addition, an analysis based on linearized unsteady aerodynamic theory was used to predict characteristics of the acoustic waves generated by the cascade.

It was found that the cascade dynamic periodicity is good for some values of interblade phase angle but poor for others. For conditions where the periodicity was good, interblade phase angle values of -45 and -90 degrees, the correlation of the data with the flat plate cascade analysis was also good. But, for the remaining values of interblade phase angle, the periodicity was poor and the data-analysis correlation was generally poor. A subsequent analysis predicted that, at interblade phase angle values of -45 and -90 degrees, the cascade produced waves which reflected off the wind tunnel upper wall in a direction away from the cascade, so that these reflected waves did not interfere with the cascade unsteady aerodynamics. At those values of interblade phase angle where the periodicity was poor, the analysis often indicated that waves were reflecting off the wind tunnel walls back into the cascade, and therefore interfered with the cascade unsteady aerodynamics.

To make this a reliable facility for the investigation of oscillating cascade aerodynamics, the effects of the wind tunnel walls must be reduced. An effort is currently under way to replace the solid tunnel walls in the vicinity of the cascade with acoustically-treated walls as developed to reduce aircraft gas turbine engine noise (Groeneweg and Rice, 1987). The effectiveness of the acoustic treatment will be investigated in part by repeating the experiments reported upon herein.

ACKNOWLEDGEMENTS

This research was supported by the Propeller and Acoustics Technology Branch and the Turbomachinery Technology Branch of the Propulsion Systems Division at the NASA Lewis Research Center. The assistance of Vincent Verhoff, Robert Olsey and Bernadette Orahoske in completion of the experiments is gratefully acknowledged.

REFERENCES

Buffum, D.H. and Fleeter, S., 1990, "Aerodynamics of a Linear Oscillating Cascade," *NASA Technical Memorandum 103250.*

Carta, F.O., 1983, "Unsteady Aerodynamics and Gapwise Periodicity of Oscillating Cascaded Airfoils," *Journal of Engineering for Power,* Vol. 105, pp. 565-574.

Groeneweg, J.F. and Rice, E.J., 1987, "Aircraft Turbofan Noise," *Journal of Turbomachinery*, Vol. 109, pp. 130-141.

Jones, W.P., 1943, "Wind Tunnel Interference Effect on the Values of Experimentally Determined Derivative Coefficients for Oscillating Airfoils," *Aeronautical Research Council Reports and Memoranda No. 1912.*

Kline, S.J. and McClintock, F.A., 1953, "Describing Uncertainties in Single-Sample Experiments," *Mechanical Engineering*, pp. 3-8.

Mehmed, O., Kaza, K.R.V., Lubomski, J.F. and Kielb, R.E., 1982, "Bending-Torsion Flutter of a Highly Swept Advanced Turboprop," *NASA Technical Memorandum 82975.*

Smith, S.N., 1972, "Discrete Frequency Sound Generation in Axial Flow Turbomachines," *Aeronautical Research Council Reports and Memoranda No. 3709.*

Whitehead, D.S., 1987, "Classical Two-Dimensional Methods," AGARD Manual on Aeroelasticity in Axial Flow Turbomachines, Volume 1: Unsteady Turbomachinery Aerodynamics, *AGARDograph No. 298*, pp. 3-1 - 3-30.

Runyan, H.L., Woolston, D.S. and Rainey, A.G., 1955, "Theoretical and Experimental Investigation of the Effect of Tunnel Walls on the Forces on an Oscillating Airfoil in Two-Dimensional Subsonic Compressible Flow," *NACA Report 1262.*

NASA
National Aeronautics and Space Administration

Report Documentation Page

1. Report No.	2. Government Accession No.	3. Recipient's Catalog No.
NASA TM-103690		

4. Title and Subtitle	5. Report Date
Wind Tunnel Wall Effects in a Linear Oscillating Cascade	
	6. Performing Organization Code

7. Author(s)	8. Performing Organization Report No.
Daniel H. Buffum and Sanford Fleeter	E-5909
	10. Work Unit No. 535-05-01

9. Performing Organization Name and Address	11. Contract or Grant No.
National Aeronautics and Space Administration Lewis Research Center Cleveland, Ohio 44135-3191	
	13. Type of Report and Period Covered: Technical Memorandum

12. Sponsoring Agency Name and Address	14. Sponsoring Agency Code
National Aeronautics and Space Administration Washington, D.C. 20546-0001	

15. Supplementary Notes

Prepared for the 36th International Gas Turbine and Aeroengine Congress and Exposition sponsored by the American Society of Mechanical Engineers, Orlando, Florida, June 3-6, 1991. Daniel H. Buffum, NASA Lewis Research Center. Sanford Fleeter, School of Mechanical Engineering, Purdue University, West Lafayette, Indiana 47907.

16. Abstract

Experiments in a linear oscillating cascade reveal that the wind tunnel walls enclosing the airfoils have, in some cases, a detrimental effect on the oscillating cascade aerodynamics. In a subsonic flow field, biconvex airfoils are driven simultaneously in harmoninc, torsion-mode oscillations for a range of interblade phase angle values. It is found that the cascade dynamic periodicity—the airfoil-to-airfoil variation in unsteady surface pressure—is good for some values of interblade phase angle but poor for others. Correlation of the unsteady pressure data with oscillating flat plate cascade predictions is generally good for conditions where the periodicity is good and poor where the periodicity is poor. Calculations based upon linearized unsteady aerodynamic theory indicate that pressure waves reflected from the wind tunnel walls are responsible for the cases where there is poor periodicity and poor correlation with the predictions.

17. Key Words (Suggested by Author(s))	18. Distribution Statement
Unsteady aerodynamics Oscillating cascade Flutter	Unclassified - Unlimited Subject Category 07

19. Security Classif. (of this report)	20. Security Classif. (of this page)	21. No. of pages	22. Price*
Unclassified	Unclassified	13	A03

NASA FORM 1626 OCT 86

*For sale by the National Technical Information Service, Springfield, Virginia 22161